The Effect of Combining Magnetic Field and High-Conductivity Nanoparticles on the Fusion Rate of a Phase Change Material

Philip Adebayo [a], Alissar Yehya [b,c] *

[a] Department of Mechanical Engineering, Maroun Semaan Faculty of Engineering and Architecture, American University of Beirut, Lebanon

[b] Department of Civil and Environmental Engineering, Maroun Semaan Faculty of Engineering and Architecture, American University of Beirut, Lebanon

[c] Harvard John A. Paulson School of Engineering and Applied Sciences, Cambridge, USA

*Corresponding author: ay36@aub.edu.lb , alissar_yehya@seas.harvard.edu (Alissar Yehya)

Abstract

In phase-change materials PCMs application for cooling, melting happens at nearly constant temperature preventing an increase in temperature until full melting occurs. So, controlling the fusion duration can be helpful to maintain the thermal comfort at lower energy demand. This study investigates the impact of using a uniform magnetic field on the rate of melting of Octadecane PCM, with and without the addition of high-conductivity nanoparticles, and when considering enclosures of various aspect ratios. We note that about 43% decrease in liquid fraction, and consequently melting rate, can be obtained for a Hartmann number of 100 and when Lorentz force direction is opposite to the buoyant force. We also show that the aspect ratio of the enclosure has an impact on the magnetic susceptibility of the PCM. Also, with the addition of nanoparticles, the effect of Lorentz force becomes more intense but the overall decrease in melting rate is not evident because of the increase in conductive heat transfer. So, their use might be promising in scenarios

23 where increasing the rate of melting is needed. Consequently, for a substantial impact on the fusion

24 rate of a phase-change material, the strength of the magnetic field, the enclosure shape, and the

25 conductivity of the material should be carefully considered.

26 **Keywords**: Phase change materials (PCM), magnetic field, numerical simulation, finite volume

27 method, melting, thermal energy storage

28 **Nomenclature**

29 $\vec{u}$ velocity vector (m/s)

30 t   time (s)

31 p   pressure (Pa)

32 $\vec{g}$ acceleration due to gravity (m/s^2)

33 T temperature (k)

34 T_{Ref} reference temperature (k)

35 T_c, T_h cold and hot wall temperature (k)

36 $\vec{D}$ Darcy source term

37 $\vec{F}_l$ Lorentz force

38 C morphology constant for the mushy region

39 b constant to prevent division by zero

40 ΔH enthalpy (J/kg)

41 L latent heat of fusion (J/kg)

42 Ha   Hartmann number

43 PCM   Phase Change Material

44 AR   Aspect Ratio

45	v	volume fraction
46	B	magnetic field strength (T)
47	E	electric field (v/m)
48	J	current density (A/m^2)
49	c_p	specific heat capacity (J/kg K)
50	k	thermal conductivity (W/m k)
51	S	heat source term
52		
53	Greek Symbols	
54	μ	dynamic viscosity (kg/m s)
55	β	thermal expansion coefficient (k^{-1})
56	σ	electrical conductivity (s/m)
57	α	liquid fraction
58	ρ	density (kg/m^3)
59		
60	Subscript	
61	s	solid state
62	l	liquid state
63	p	nanoparticle
64	nf	nano enhanced PCM
65		
66		
67		

1. Introduction

Phase change materials, used as latent thermal energy storage means, are gaining prominence in energy storage applications due to their important roles in energy technologies [1]. Mainly, phase change materials have high latent heat of fusion and can store and release heat at a nearly constant temperature. Consequently, they can improve temperature regulation and reduce energy consumption – thus contributing to the reduction of CO_2 emissions [2], [3]. They are applied in solar energy storage, smart housing, agricultural greenhouses, temperature-regulating textile, heat management of electronics, telecommunications, microprocessors, and biomedical systems [4]. Latent heat storage systems are also used in building envelopes, household hot water supply systems, domestic space heating and air conditioning, and absorption refrigeration [5].

Nevertheless, the use of phase change materials for energy storage suffers from major drawbacks. They, generally, have poor thermal conductivity [6], show incongruent melting, and exhibit large supercooling Hirschey et al. [7]. Dannemand et al. [8] also highlighted the problem of phase separation, expansion, and contraction of phase change materials during melting and solidification and impulsive release of heat.

Several research groups have developed strategies to resolve some of these downsides. Xie et al. [9] proposed the use of nucleating agents in resolving the issue of supercooling and the use of porous materials to address the problem of leakage, phase separation, and corrosion of phase change materials.

On the other hand, in most applications, phase-change materials lack control on determining when energy should be released because their crystallization depends on the ambient temperature [10]. To avoid this, a high energy barrier for reverse-phase change from high to low energy must be

4

91   installed [11]. Intermolecular forces such as Vander Waals, dipolar, and hydrogen bonding

92   influence phase shifts, and transition temperature and heat storage density can be adjusted by

93   modifying the main interactions between constituents [12] [13].

94   Another issue that is not tackled in the literature is how fast the PCM stores and releases the energy.

95   Most works [20-22] focused on improving heat transfer by improving the thermal conductivity pf

96   the PCM through the addition of nanoparticles. They found out that adding conductive

97   nanoparticles to PCM enhance heat storage rate and power [20-22] and can hamper convective

98   heat transfer [21]. However, in some applications it might be helpful to reduce the rate of melting

99   to extend the duration of fusion. In cooling of buildings, for example, as the external temperature

100   increases, the building envelope is responsible for delaying the transfer of heat to the inside. When

101   PCMs are used, they store the excess heat as they melt and avoid the increase in room temperature

102   (increase thermal capacity of the envelope). After fully melted, the PCM will act as any other

103   medium with low conductivity. Hence, they are mostly effective when they are undergoing a

104   phase-change. In such case, it is useful to extend the duration of phase-change by reducing the rate

105   of melting. The rate of melting at which the PCM melts depends on the temperature gradient

106   between the surrounding and the PCM. In this work, we investigate the potential of using a

107   magnetic field as a mean to reduce the rate of fusion.

108   Zhang and Nawaz [14] used a magnetic field to control the temperature of a thermal management

109   system made up of PCM and magnetic particles coated on the shell. They discovered that magnetic

110   particles boost thermal conductivity and that the magnetic force improves heat transmission

111   between the PCM and the heat source. Goncalves et al. [15] used the enthalpy approach with

112   Lorentz force to include the magnetic field effect and model the melting process of a phase-change

113   material. They reported a flow field distortion due to the strong magnetic field effects, which

114   resulted in further melting due to interface erosion.

115   Using a two-phase mixture model, Yousefi et al. [16] investigated the influence of a non-uniform

116   magnetic field on forced convection heat transfer in a flattened tube. Due to the creation of kelvin

117   body forces and growing gradients of velocity and temperature near the tube wall, the non-uniform

118   magnetic field influences the flow and causes an increase in heat transfer, according to the

119   numerical results. Mehryan et al. [17] investigated the melting behavior of phase-change materials

120   in a cavity subjected to a non-uniform magnetic field using a moving grid approach and Lorentz

121   force as a source term. At the beginning of the melting process, they found no substantial effect

122   on natural convection. The velocity of the fluid, as well as the influence of the magnetic field,

123   increased as the melting front advanced and the liquid fraction increased.

124   Using the enthalpy porosity model and the Lorentz force as a source term in the momentum

125   equation, Doostani et al. [18] explored the influence of the presence of a uniform magnetic field

126   on the rate of melting and melting behavior of an electrically conducting material in a cavity

127   (gallium). They discovered that increasing the Hartmann number slows down the phase-change

128   process and that the presence of a uniform magnetic field affects the melting front and regulates

129   flow velocity. Moreover, Selimefendigil and oztop [19] investigated how a magnetic field and

130   hybrid nanoparticles affected the thermal performance of a phase-change energy system, using an

131   artificial neural network and a finite element approach. They noticed a faster phase transition near

132   the wall and reported a reduction in charging time with the imposed magnetic field.

133   The discussed literature shows the potential for magnetic field and nanoparticles to impact the

134   phase-change process. However, there is still a lack of studying this effect on passive building

135   envelopes. Hence, in our work, we use a low conductivity phase-change material, Octadecane, a

136 hydrocarbon that is widely used in building envelopes, and we try to understand the design factors

137 that improve the susceptibility of the material to magnetic field. We investigate the effect of using

138 magnetic field, with and without adding nanoparticles to the PCM, in controlling the energy

139 storage process during melting. We also study the effect of the aspect ratio of the enclosure on the

140 PCM's susceptibility to magnetism. We model the effect of magnetic field by including the

141 Lorentz force as a source term in the momentum equations, which are fully coupled with the energy

142 equations.

143 The rest of this paper is structured as follows: Section 2 is devoted to the discussion of the

144 governing equation and problem description. In section 3, we discuss benchmark cases from the

145 literature for validation of the numerical model. In section 4, we present thorough analysis of the

146 numerical simulation and the main results. Finally, section 5 brings the paper to a close by

147 presenting key findings.

148 **2. Numerical Model**

149 **2.1. Governing Equations**

150 For numerical studies of phase-change materials, accurate prediction of melting rates is essential

151 to ensure optimal performance of a latent heat thermal storage device [2], [23], [24]. This depends

152 on a numerically robust mathematical model based on the continuity, momentum, and energy

153 equations during the phase change process. The mathematical model using the enthalpy-porosity

154 method was implemented in OpenFOAM, an open-source Computational Fluid Dynamics toolbox

155 based on a finite volume method. Viscous dissipation as well as radiation are considered

156 negligible. The flow is assumed to be laminar and incompressible and boussinesq approximation

157   is adopted. The governing equations of the model include coupling the continuity equation with

158   the momentum and energy equations to solve for the temperature and velocity fields.

159   The continuity equation for an incompressible fluid is:

160    $\nabla . \vec{u} = 0$ (1)

161   The momentum equation is expressed as,

162    $\rho \frac{\partial \vec{u}}{\partial t} + \rho(\vec{u}.\nabla)\vec{u} = -\nabla p + \mu\nabla^2\vec{u} + \rho\vec{g}\beta(T - T_{Ref}) + \vec{D} + \vec{F_l}$ (2)

163    $\vec{u}$ is the velocity vector, p is the pressure, ρ is the density, g is the acceleration due to gravity, μ is

164   the dynamic viscosity, β is the thermal expansion coefficient, T is the temperature and T_{Ref} is the

165   reference temperature. $\vec{D}$ is the Darcy source term which makes the momentum equations match

166   Carman-Kozeny equation for flow in porous media as used by Brent et al. [25]. The equation is

167   expressed in Eq. (3). $\vec{F_l}$ is the force due to the magnetic field, which is adapted from [17, 18] and it

168   is based on simplification from the electric transfer equation. The force is described in Eq. (5).

169    $\vec{D} = -C \frac{(1-\alpha)^2}{\alpha^3+b} \vec{u}$ (3)

170   where C is the constant that accounts for the morphology of the mushy region; b is a constant that

171   prevent division by zero and has been taken to be 1 x 10^{-3} in the literature.

172   α is the liquid fraction and it is defined as below using the approach of [20,21].

173    $\alpha = \frac{\Delta H}{L} = \begin{cases} 0 & T < T_s \\ \frac{T-T_S}{T_l-T_S} & T_l < T < T_s \\ 1 & T > T_l \end{cases}$ (4)

174   T_l and T_s are the liquidus and solidus temperature of the PCM, respectively. ΔH is the latent heat.

175   L represents the latent heat of fusion of the phase change material.

176   The Lorentz force is expressed as,

177      $$F_l = \sigma B^2\, u_y \tag{5}$$

178   where σ is the electric conductivity and B is the magnetic field strength and u_y is the velocity in

179   the vertical direction (i.e. parallel to the gravitational acceleration). The non-dimensional

180   Hartmann number can be written as:

181   $$Ha = L_y B \sqrt{\frac{\sigma}{\mu}} \tag{6}$$

182   The Energy Equation is expressed as,

183   $$\rho c_p \frac{\partial T}{\partial t} + \rho c_p (\vec{u}.\nabla T) = k\nabla^2 T + S \tag{7}$$

184   c_p is the specific heat capacity and k is the thermal conductivity. Density, heat capacity and thermal

185   conductivity are defined using linear relationship between their corresponding solid and liquid

186   values and are expressed in Eq. (8) - (10), respectively. c_{pl} and c_{ps} are the heat capacity in the

187   liquid and solid state of the pcm. Similarly, k_l and k_s are the thermal conductivity of the pcm in

188   its liquid and solid state. S is the source term due to the latent heat and can be calculated using

189   equation (11).

190   $$\rho = \alpha \rho_l + (1 - \alpha)\rho_s \tag{8}$$

191   $$c_p = \alpha c_{pl} + (1 - \alpha)c_{ps} \tag{9}$$

192   $$k = \alpha k_l + (1 - \alpha)k_s \tag{10}$$

193    $S = -L\rho(\frac{\partial \alpha}{\partial t} + \nabla.(\alpha \vec{u}))$ (11)

194   **2.2. Modelling of nanoparticles**

195

196   To study the effect of addition of nanoparticles on phase change material, we will be employing

197   the Brinkman and Maxwell model for nanofluid [28] [29]. The effective thermal conductivity is

198   defined as:

199    $k_{nf} = k \left[\frac{(k_p + 2k - 2(k - k_p)v_p)}{k_p + 2k + (k - k_p)v_p} \right]$ (12)

200   where $k_{nf}, k, k_p \; and \; v_p$ are the thermal conductivity of nanofluid, pure PCM, magnetite and

201   volume fraction of magnetite, respectively. The effective viscosity can be written as:

202    $\mu_{nf} = \frac{\mu}{(1 - v_p)^{2.5}}$ (13)

203   μ_{nf} is the dynamic viscosity of the nanofluid while μ is the viscosity of the PCM. The density of

204   the resulting nanofluid can be computed using the relation defined as below

205    $\rho_{nf} = (1 - v_p)\rho + v_p \rho_p$ (14)

206   ρ_p, ρ, ρ_{nf} are the density of the magnetite, pure PCM and nanofluid, respectively. Effective heat

207   capacitance is defined as:

208    $(\rho c_p)_{nf} = (1 - v_p)\rho c_p + v_p (\rho c_p)_p$ (15)

209    $(\rho c_p)_p, (\rho c_p)_{nf}, \rho c_p$ are the heat capacitance of magnetite, nanofluid and pure PCM,

210   respectively. The effective thermal expansion coefficient can be defined as:

211    $(\rho \beta)_{nf} = (1 - v_p)\rho \beta + v_p (\rho \beta)_p$ (16)

212

213    $\rho\beta, (\rho\beta)_p$ are the thermal expansion volume of pure PCM and magnetite, respectively. The

214   latent heat of the nanofluid can be written as:

215    $(\rho L)_{nf} = (1 - v_p)\rho L$ (17)

216   where ρL is the latent heat of pure PCM.

2.2. Problem Description

218   Figure 1 shows a two-dimensional configuration of the physical model. The phase change material

219   used in this study is octadecane because its melting temperature belongs to the building thermal

220   comfort temperature range [2]. The left and right walls of the cavity are at constant temperatures

221   T_H and T_C, respectively, while the top and bottom walls are insulated. No slip velocity boundary

222   conditions are employed at the left and right walls of the cavity and a uniform magnetic field is

223   applied to the vertical walls.

Insulated wall

$$\frac{\partial T}{\partial x} = 0$$

Hot wall

$\vec{B}$

$\vec{g}$

Cold wall

Ly

$T = T_H$
U=0
V=0

$T = T_C$
U=0
V=0

$$\frac{\partial T}{\partial x} = 0$$

Insulated wall

Lx

224
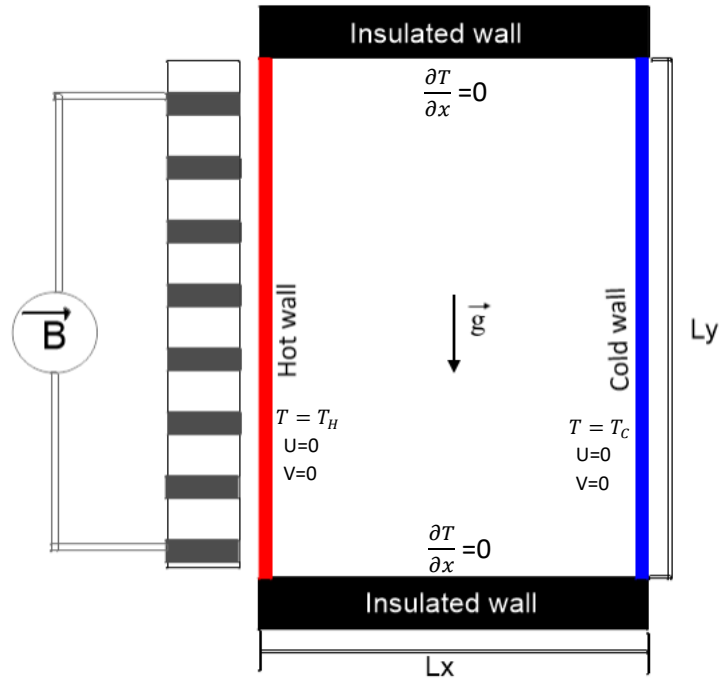
Figure 1:Schematic Diagram of the Physical Model showing the geometry and the boundary

conditions

3. Validation of the Numerical Model

Before extensive discussion of the result, it is important to check the accuracy of our model with

other reported results in the literature. For this purpose, we compare the results of our model with

two benchmark cases from [18], [27]. The properties of the materials used in the simulations are

gathered in Table 1.

Table 1: Thermophysical Properties of Gallium and octadecane

Parameters	Gallium [17]	Octadecane [22]
Density (kg.m⁻³)	6093	867 (solid)
		775.6 (liquid)

Latent Heat (J.g^{-1})	80.160	243.680
Melting Temperature (K)	302.85	301.15
Thermal Conductivity (W.m^{-1}. k^{-1})	32	0.32 (solid)
		0.15 (liquid)
Specific heat (J. kg^{1}. K^{-1})	381.5	1900 (solid)
		2240 (liquid)
Kinematic viscosity (m^2.s^{-1})	2.97 x 10^{-7}	4.81 x 10^{-6}
Thermal Expansion coefficient (K^{-1})	1.2 X 10^{-4}	8.36 x 10^{-4}

233

234   The first comparison is with the work of Doostani et al. [17], which numerically studied the effect

235   of magnetic field on melting of gallium in a square enclosure of side 6.35 cm using non

236   dimensional Hartman number 0, 30, 50, 70 and 100. The hot wall and the cold wall are maintained

237   at 38°C and 28.3°C, respectively, while the top and bottom walls are insulated. It is noteworthy to

238   say that the decision to compare the findings of Doostani et al. [18] with the current work is

239   because they did an extensive model validation with popular or most used experimental and

240   numerical models in the literature for the case of melting of gallium without magnetic effect and

241   had good agreement. The thermophysical properties of gallium are listed in Table 1. Several

242   investigations were conducted to determine the appropriate grid size and time step. A grid size of

243   150x150 and time step of 2s were sufficient to give accurate result. Morphology constant of the

244   mushy region is as well important to accurately predict the melting interface. In this case,

245   morphology constant of 10^6 kg/m^{3}s was used for melting of gallium. Figure 2 show the

246   comparison of the position of the melting front reported by the reference and the current model for

247   the melting of gallium for different Hartmann numbers and at 120, 300, 600 and 1140s. The results

248   are in close agreement for all cases.

249

(a)

(b)

(c)

(d)

15

(e)
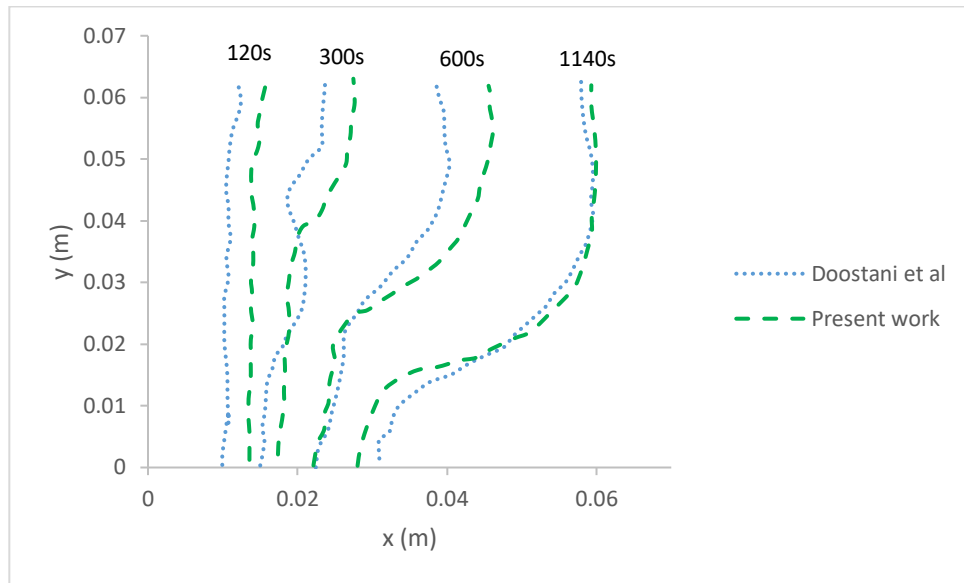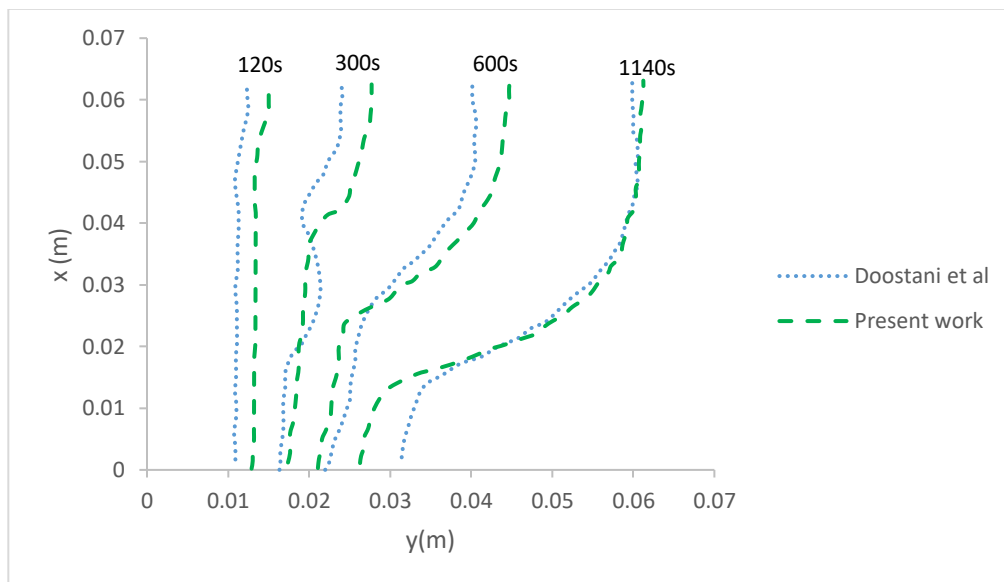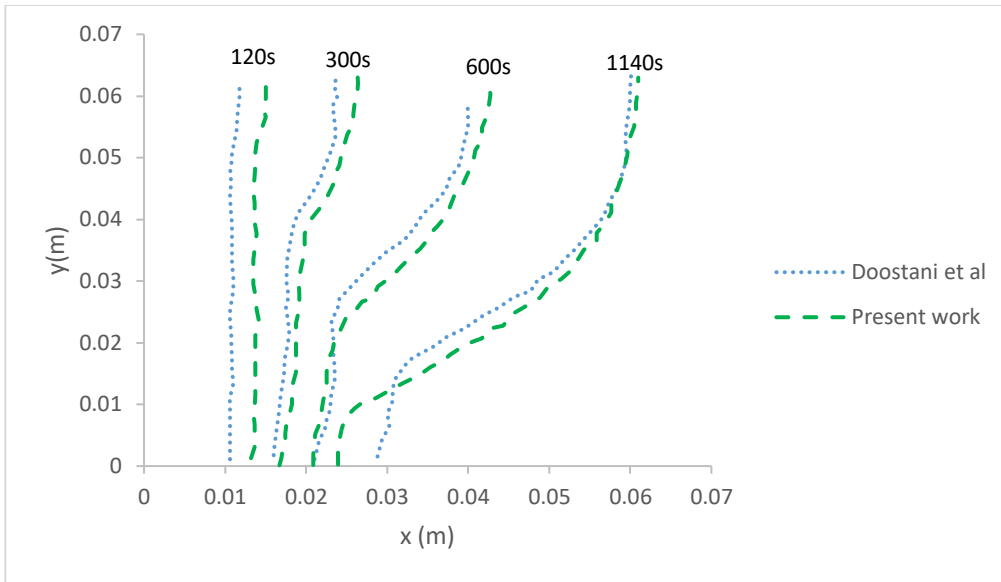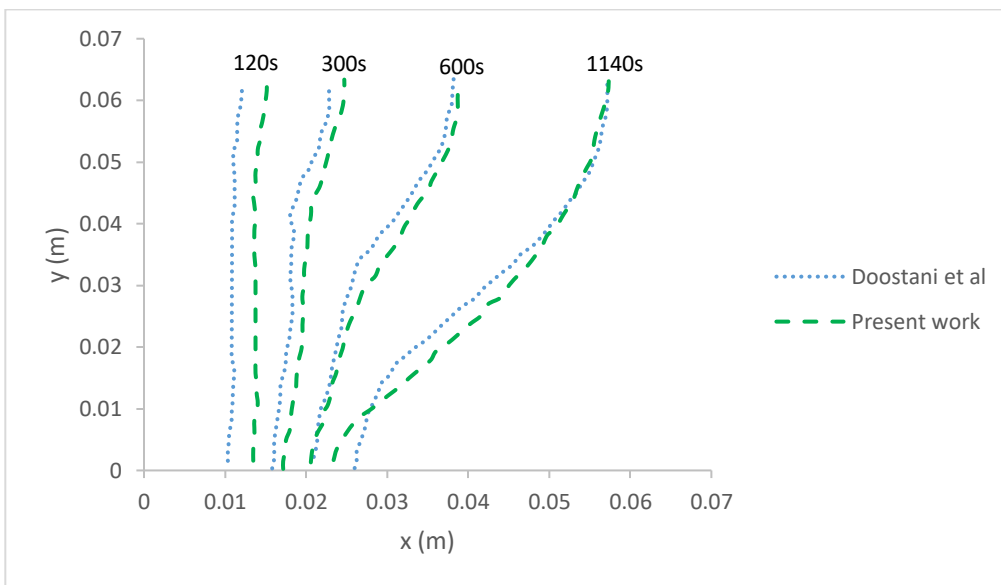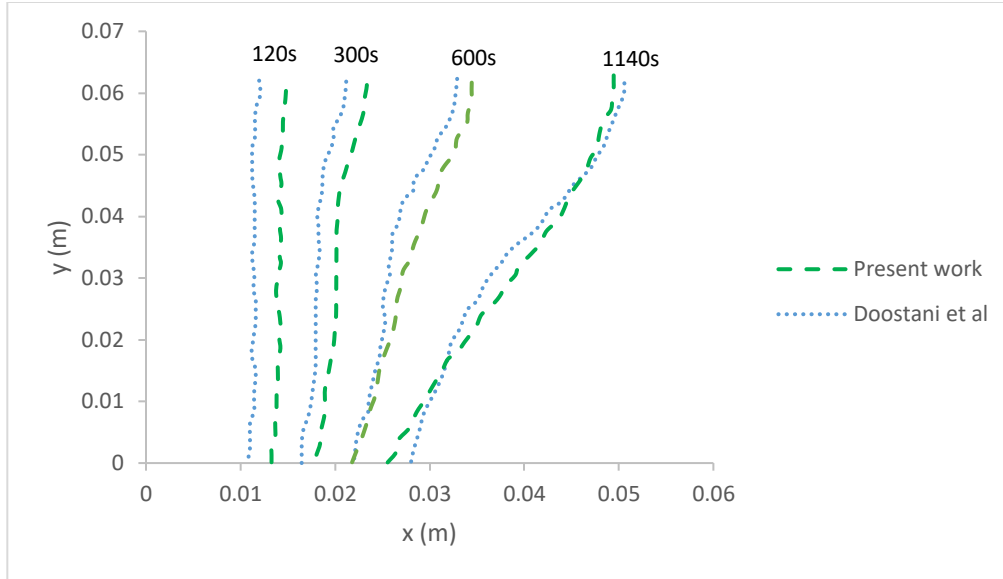
Figure 2: Position of the melting interface from the present work compared to the work of

Doostani et al. (2017) for (a) Ha=0 (b) Ha=30 (c) Ha=50 (d) Ha =70 and (e) Ha=100

Furthermore, the results of our simulation have also been compared with the work of Faden et al

[30], which is a two-dimensional problem of melting of octadecane in a square cavity of length 40

mm. Again, the decision to benchmark our result with Faden et al. [30] is because of the extensive

validation of their model with experimental findings. In this case, the hot and cold walls are at

constant temperature 308.15 K and 298 K, respectively. The thermophysical properties of

octadecane are presented in Table 1. Also, we carried out several investigations to determine the

precise grid size, time step and morphology constant. Grid size of 400x400, time step of 2s and

morphology constant of 10^7 kg/m^{3}s give accurate results. The melting front after 1h, 2h, 3h and 4h

of the simulation time are plotted in figure 3 and compared with the result of Faden et al [30]. It

can be observed that the comparison of the present work with the reference is favorable with slight

incongruity. At all reported simulation times, there is a very good agreement at the bottom of the

cavity, but the slight incongruity can be observed at the top of the cavity. This could be due to the

264 differences in the method used in discretizing the convection term and the momentum-energy

265 equation coupling as well as the use of extended domain by the reference.

266
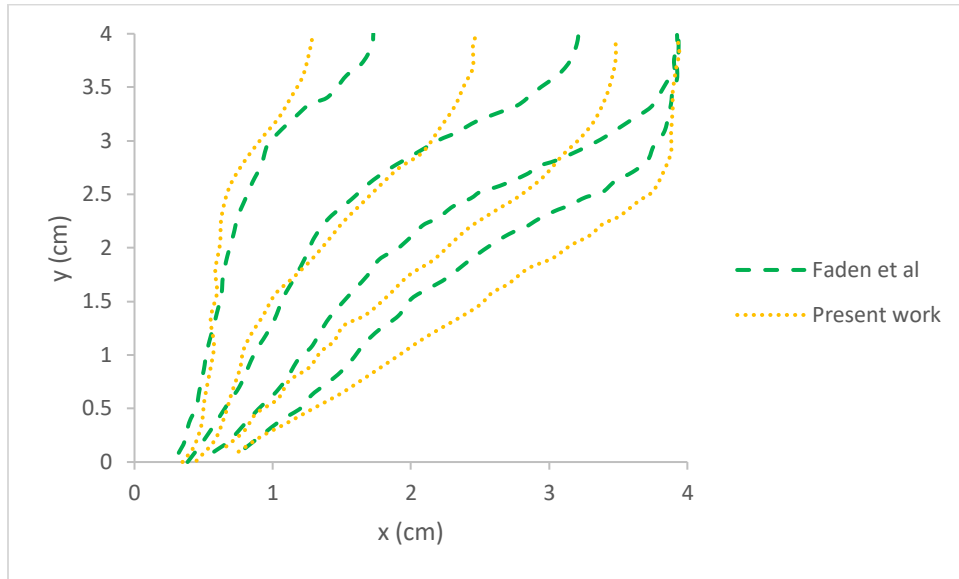
267

268 *Figure 3: Position of the melting interface from the present work compared to the work of Faden*

269 *et al. (2019)*

270 In summary, a close agreement exists between our model and previous reported work in the

271 literature for both magnetic and without magnetic field. This further proves the validity of the

272 present numerical results.

273 **4. Results and Discussion**

274 In this section, we discuss the effect of magnetic field on melting process of Octadecane in an

275 enclosure, building on the validated test case of Faden et al [30] The non-dimensional Hartmann

276 number is affected by three factors: magnetic field strength, conductivity and enclosure geometry.

277 Therefore, to improve the susceptibility of the PCM to magnetism, the effect of different magnetic

278 field strength, enclosure geometry and nanoparticles are investigated.

279 **4.1. Effect of Magnetic Field on Melting of Octadecane in a Square Enclosure**

280 In the previous section, we compared present result for the melting of octadecane in a square

281 enclosure of length 40 mm with the literature. Now, the effect of magnetic field on the melting

282 process will be discussed using the non-dimensional Hartman number 0, 20, 60 and 100. Figure 4

283 shows the melting front at different Hartman numbers and times. Figure 4a shows the melting front

284 for various Hartmann numbers after 1hour of simulation time. At the beginning of the simulation,

285 it is assumed that the Octadecane is completely solid, and the primary mode of heat transfer is

286 conduction. The magnetic field has no effect at the bottom of the enclosure, but at the top of the

287 enclosure, we observe a decrease in the progression of the melting front. This is more evident at a

288 higher Hartman number, which shows that the increase in Hartman number can affect the melting

289 process. As expected, the fluid motion deteriorates as a result of the role of the magnetic field. The

290 shape of the melting front is affected by natural convection, which makes the front move faster at

291 the top than the bottom of the enclosure [31].

292 Likewise, figures 4(b)- (d) show the plot of melting interface for various values of Hartmann

293 number at the simulation time of 2-4 hours, respectively. Unlike at the simulation time of 1 hour,

294 it can be observed that the magnetic field effect is not only felt at the top of the enclosure but also

295 at the middle of the enclosure. Apparently, lower magnetic field does not have a noticeable effect

296 on the melting process but as the magnetic field becomes stronger the impact can be seen.

297 The magnetic field can impact the convective flow. This has a corresponding effect on the

298 progression of the melting interface and the rate of melting. Figure 5 shows the plot of the average

299 liquid fraction with time. Up to about 1 hour of the simulation time, there is no significant effect

300 of the magnetic field on the melting rate. This could be because of the dominant heat transfer

301 mechanism being conduction. As the melting progress and there is increase in convective flow,

302 the effect of magnetic field on the melt fraction can be observed. At the maximum simulation time

303 of 4 hours, we notice about 43% decrease in melted fraction at the maximum Hartmann number

304 investigated. We can conclude that higher magnetic field impacts the rate of melting.

(a)

(b)

(c)

(d)
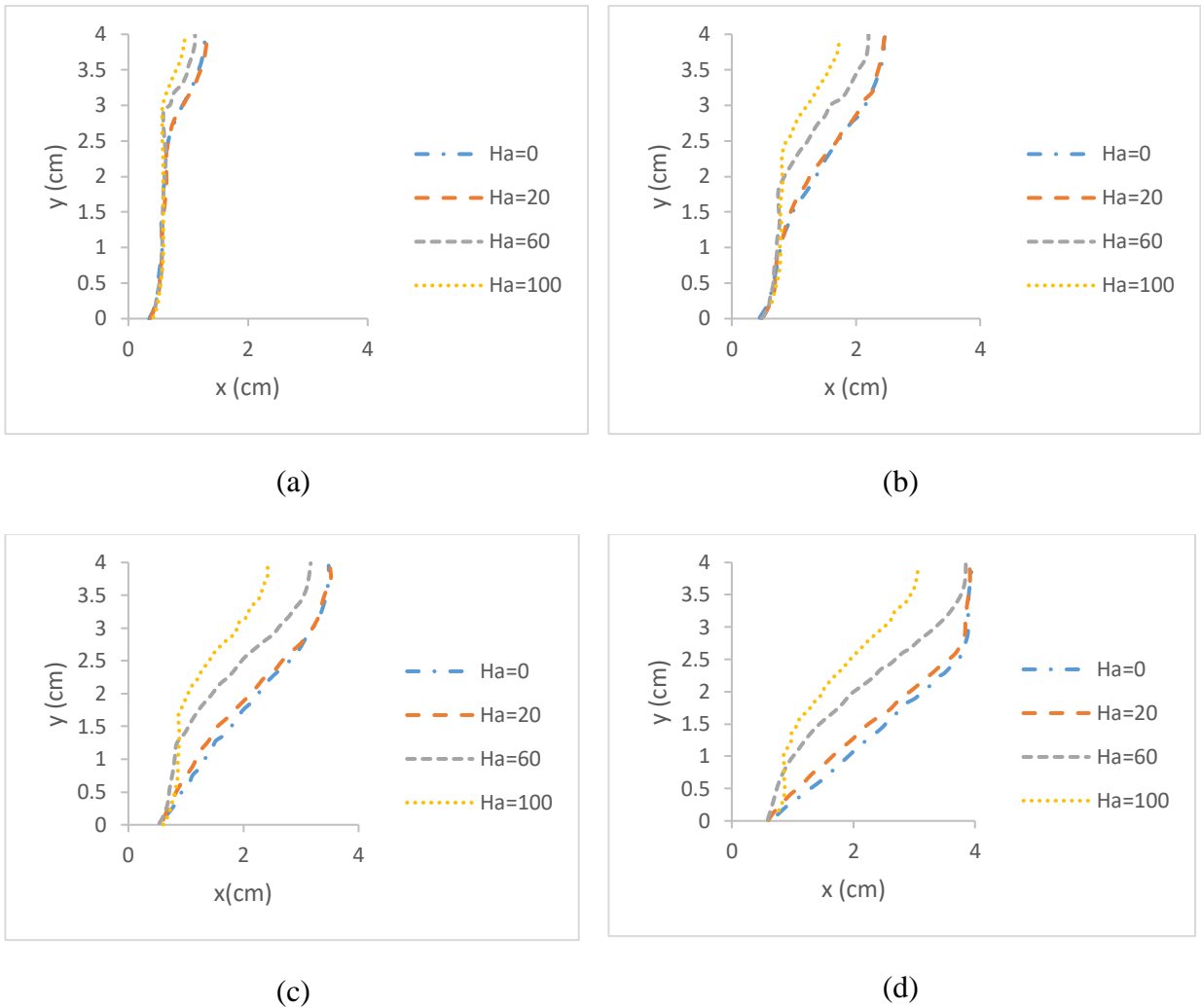
305 *Figure 4: Position of the melting interface for various Hartmann numbers and different times:*

306 *(a)1hour (b)2 hours (c) 3hours and (d) 4 hours*

307
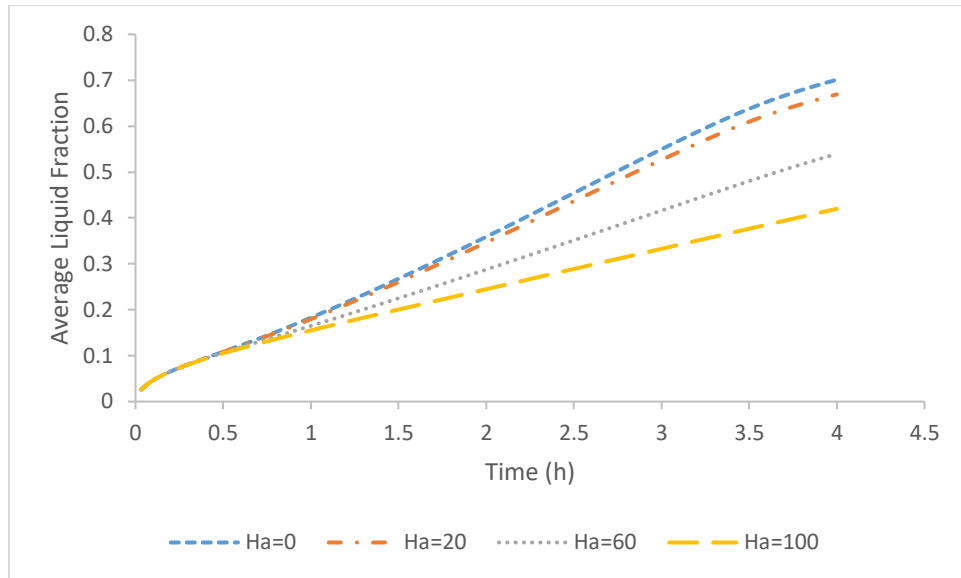
Figure 5: Average liquid fraction versus time plotted for various Hartmann numbers

308

4.2. Influence of Enclosure Aspect Ratio

309

310   To further deepen the understanding of the impact of magnetic field on melting of Octadecane,

311   numerical simulation was conducted for rectangular enclosures with different aspect ratios. The

312   shape of enclosure has been shown to affect heat transfer and thermal losses [32], [33] [[34]. The

313   investigation will help us to determine the best enclosure design, which can be influenced by the

314   magnetic field. This was achieved by keeping the area of the cavity constant as in the square cavity

315   discussed in the previous section, which signifies that the quantity of PCM remains the same. We

316   consider cavity sizes of 5x3.2, 3.2x5, and 2x8 with equivalent aspect ratio 0.64, 1.56 and 4,

317   respectively, at a constant magnetic field strength equivalent to the Hartmann number of 60 in the

318   square enclosure. Figure 6 shows the plot of liquid fraction with time for various enclosure aspect

319   ratios considered in our study without the influence of magnetic field magnitude. We would like

320   to reiterate that our aim is to be able to control the rate of melting to control the spontaneous heat

321   release or stored during phase change process. As shown in figure 6, enclosure geometry can also

322 help in achieving this. It can be observed that a horizontally oriented (the longer side is parallel to

323 x-axis) rectangular enclosure with the aspect ratio of 1.56 gives the melting fraction with the lower

324 melting rate for all the considered geometry. On the other hand, the vertically oriented (the longer

325 side is parallel to y-axis) rectangular enclosures with aspect ratio 4 gives the highest melting rate.

326 For thermal storage design where low melting rate is desired, an enclosure design with lower aspect

327 ratio where the thickness is longer than the width will be ideal.

328 The magnetic field effect is also influenced by the enclosure geometry and the comparison is

329 presented in figure 7. For all investigated geometries, the presence of magnetic field causes a

330 reduction in the melting rate. Again, the enclosure with the lower melting rate is the cavity size

331 with aspect ratio 1.56. Figure 8 shows the plot of the total liquid fraction at the end of simulation

332 time of 4 hours for both no-magnetic field and magnetic field. It can be pointed out that the

333 presence of magnetic field causes a reduction of about 23% in the melted fraction for the cavity

334 size with aspect ratio 0.64 while about 24.8% for cavity size with aspect ratio 1.56. Similarly, a

335 reduction in the melted fraction of about 18.7% for aspect ratio of 4 while for the square cavity

336 size of length 4cm (aspect ratio of 1) recorded about 23% decrease in the melted fraction.

337

338
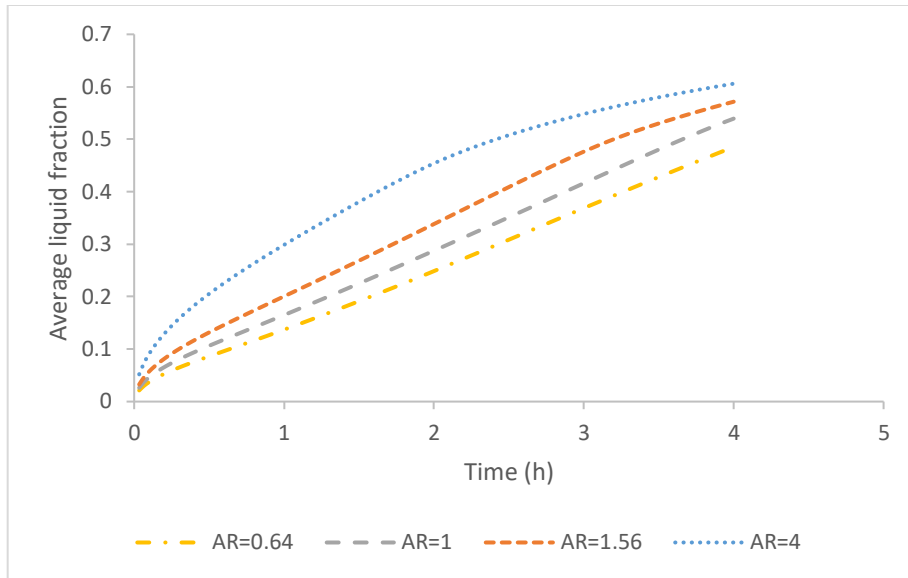
Figure 6: Average liquid fraction versus time plotted for different aspect ratios in the case where

there is no magnetic field

341
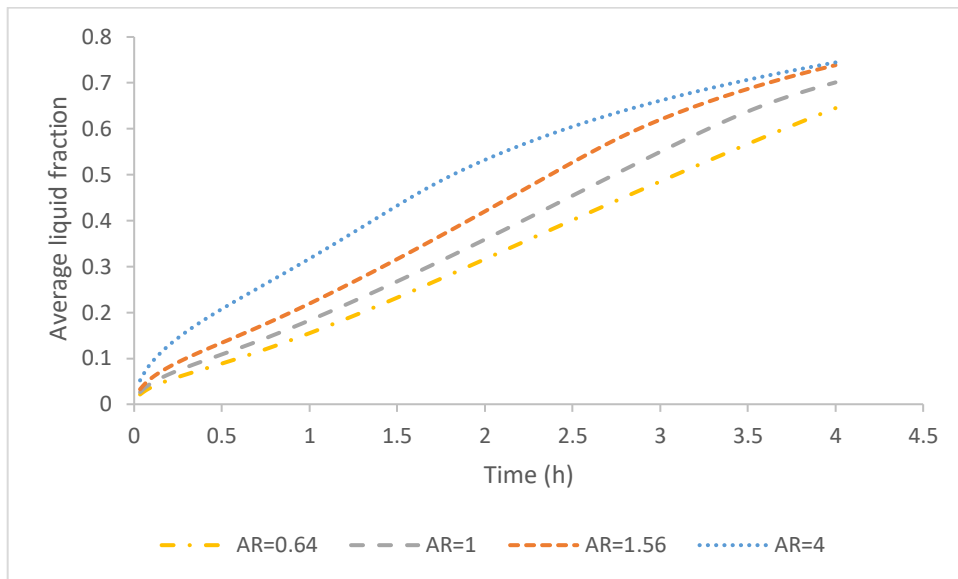
Figure 7: Average liquid fraction versus time plotted for different aspect ratios for the same

magnetic field strength
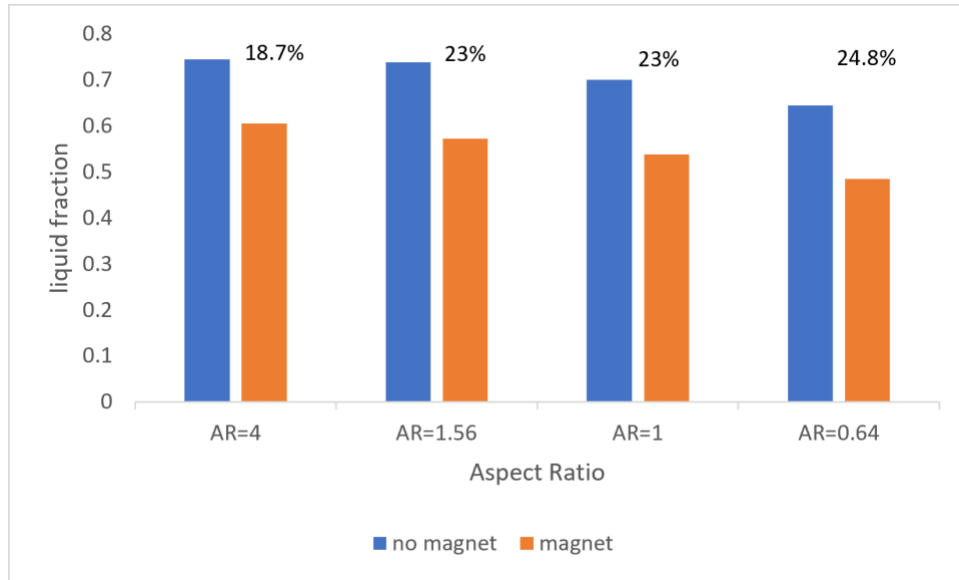
Figure 8: Summary for the comparison of the liquid fraction at the end of the simulation time of 4 hours for different aspect ratios for the two cases: with and without magnetic field

4.3. Effect of Nanoparticles on the Melting Process of Octadecane in a square enclosure

Nanoparticles with high thermal conductivity has been reported to enhance the thermal conductivity of phase change materials [22] . In this study, we examine the role of nanoparticles on the melting process of octadecane using Copper Oxide and Aluminum oxide at a volume fraction of 6%, 10% and 14%.

355 *Table 2: Thermophysical Properties of Nanoparticles*

Properties	CuO [21]	Al$_2$O$_3$ [35]
Thermal Conductivity (W/m K)	18	36
Specific heat (J/kg K)	540	765
Density (kg/m^3)	6510	3600
Thermal expansion coefficient (1/K)	1.67x10^{-5}	NA

356

357　The thermophysical properties of the considered nanoparticles is presented in Table 2. The

358　variation of liquid fraction with time for various nanoparticle fraction is presented in figure 9. For

359　about 1 hour of the simulation time, there is no significant influence of the nanoparticle on the

360　fraction of the melted PCM.　　However, at about 2 hours, there is a significant effect of the

361　nanoparticles on the melting fraction. It can be observed that as the volume of the nanoparticles

362　increased, the fraction of the melted phase change material increases. This implies that at the

363　highest nanoparticle volume fraction investigated, the melting progress faster and the liquid

364　fraction increased significantly at the end of the simulation time. The observable increase in the

365　melting rate could be attributed to the enhancement of the effective thermal conductivity of the

366　PCM because of the higher thermal conductivity of the nanoparticles used. Comparing the two

367　nanoparticles investigated, we could see that there is no significant difference in their effect when

368　compared with the pure phase change material. This point out the fact that the higher thermal

369　conductivity of the nanoparticles is not the only factor affecting the enhancement of the melting

370　rate. Higher density of the nanoparticles as well as effective viscosity also influence the

371   enhancement. In the process of selecting nanoparticle for enhancement of phase change material,

372   it calls for extra care to ensure that the thermophysical properties balances well with the PCM for

373   optimal benefit.
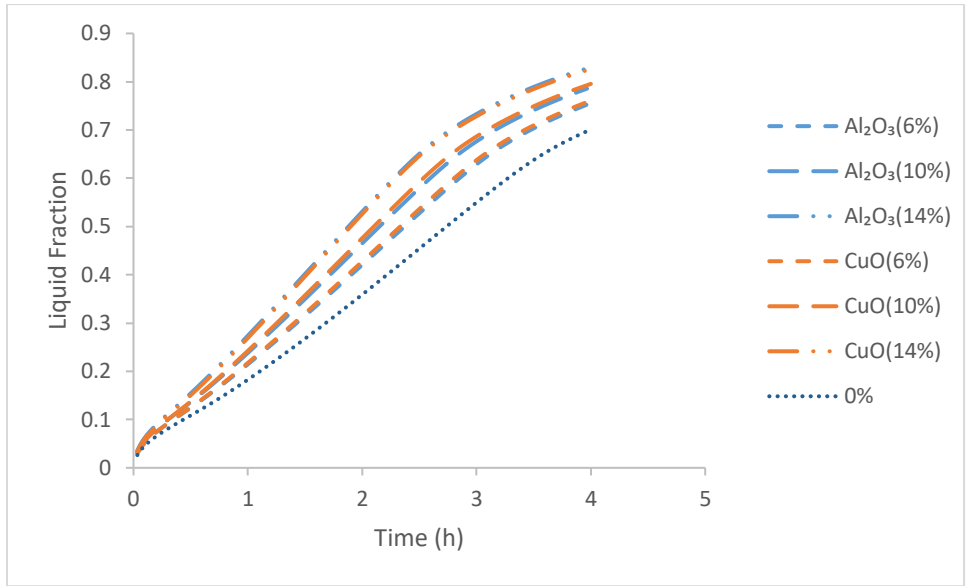
374

375   *Figure 9: Average liquid fraction versus time for different nanoparticles and volume fractions for*

376   *the case without magnetic field*

377

378   **4.4. Effect of Magnetic Field on the melting Performance of Nanoparticle enhanced**

379   **Octadecane**

380

381   In the previous section, we have been able to establish that the use of nanoparticles enhances the

382   melting rate of PCM. Several research groups have considered the use of nanoparticle enhanced

383   phase change materials for thermal storage. Therefore, it is important to also study the effect of

384   magnetic field on nanoparticle enhanced phase change materials. For this purpose, we subjected

385   the enhanced PCM to a magnetic field strength with the Hartmann number 60. Figure 10 shows

386 the plot of the melting fraction variation with time for different volume fractions of Aluminum

387 oxide under magnetic field effect. Initially, from figure 9, the use of 6%, 10% and 14% volume

388 fraction of Al_2O_3 resulted in melting fraction increase of about 9%, 13% and 19%, respectively at

389 the end of the simulation time. Now with the external magnetic field acting on the nano-enhanced

390 phase change material, we observed decrease in the melted fraction of the PCM. Compared with

391 the nano enhanced PCM without magnetic field, there's about 21% decrease in the melted volume

392 fraction for all nanoparticle volume fraction investigated.

393 Similarly, in figure 11, we presented the plot comparing the magnetic field effect on the

394 nanoparticle enhanced phase change material at different volume fraction. We observed that with

395 6% volume fraction, there is about 22% decrease in the melting fraction while 21% and 20% for

396 10% and 14% volume fraction of CuO nanoparticle, respectively. In previous section, we reported

397 about 23% decrease in the melting fraction under the same magnetic field effect without the use

398 of nanoparticle. We can conclude that, the use of nanoparticle under magnetic field may not be so

399 economical and rewarding for a system where low melting rate is so desired. However, for a system

400 where faster melting is important, the use of nano-enhanced phase change material without

401 magnetic field could be a better option.

402
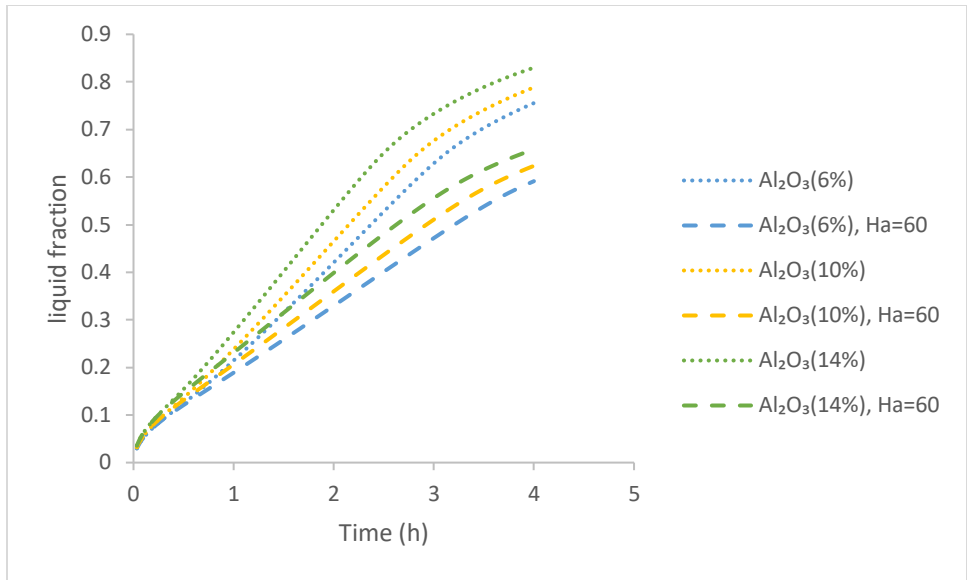
Figure 10: Average liquid fraction versus time for various volume fractions of Al_2O_3 under

magnetic field effect with Ha=60

405
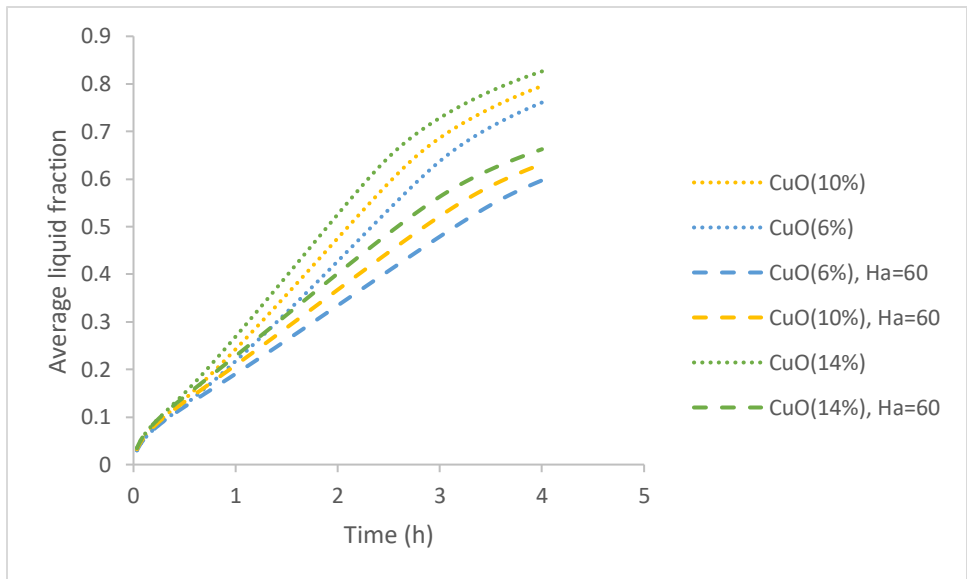
Figure 11: Average liquid fraction versus time for various volume fractions of CuO under

magnetic field effect with Ha=60

5. Conclusion

409 For an efficient performance of phase-change materials (PCM)s in thermal energy storage systems,

410 the time needed for the fusion process should be well coordinated with the duration of external

411 heating and cooling. Thus, it is important to investigate methods to control the melting of PCMs.

412 In this work, we investigated how magnetic field affects the fusion rates of Octadecane. The results

413 can open the door for designing systems where the PCM fusion is controlled depending on the

414 expected external heating and cooling rates.

415 The effect of magnetic field on the melting of PCMs depends on the magnitude of the field, the

416 PCM properties, and the enclosure geometry. This is inferred from the decrease in rate of melting

417 as the Hartman number increases, up to 43% for the maximum investigated magnetic field when

418 Lorentz force is directed opposite to the buoyant force. As the magnitude of the magnetic field

419 applied on the vertical side of the enclosure increases, the rate of melting decreases and this

420 becomes more evident as the melting front proceeds and as convection's contribution becomes

421 stronger. Besides increasing the magnetic field magnitude, the Hartman number can be increased

422 by improving the conductivity of PCM using nanoparticles or increasing the height of the

423 enclosure. For a constant magnetic field magnitude and constant PCM quantity, i.e. constant

424 volume of enclosure, the aspect ratio of the cavity influences the degree of effect of the magnetic

425 field. From here, we conclude that designing PCM enclosures of optimal aspect ratios allows for

426 a higher effect of the same magnetic field. Also, the choice of the magnetic field strength will

427 depend on the intended reduction in fusion rate. On the other hand, adding nanoparticles increases

428 the Lorentz force but the overall decrease in melting rate is not evident because of the increase in

429 conductive heat transfer. So, their use might be promising in scenarios where increasing the rate

430 of melting is needed.

431 This study has some limitations. The numerical model takes considers the effect of magnetic field

432 through adding the Lorentz force. While this approach has been used in the literature, we think

433 that there can be another effect of magnetic through improving the heat capacity of the PCM or

434 causing a change in the onset of melting. The hypothesis is that there are two competing

435 phenomena that might control the effect of magnetic field on the fusion of the PCM. The first is

436 related to the Lorentz force that affects the convection of the material and is considered here, and

437 the second is related to the effect of magnetic field on the binding energy of the material. There is

438 no work in the literature that has experimentally considered this effect for PCMs. Future work will

439 include experimental validation and improvement of the numerical model to account for the two

440 effects.

Disclosure Statement

446 The authors declare no conflict of interest.

References

448 [1]   C. Pan, S. Hoenig, C. H. Chen, S. Neti, C. Romero, and N. Vermaak, "Efficient modeling of
449   phase change material solidification with multidimensional fins," *Int J Heat Mass Transf*,
450   vol. 115, pp. 897–909, 2017, doi: 10.1016/j.ijheatmasstransfer.2017.07.120.

451 [2]   A. Yehya, H. Naji, and L. Zalewski, "Experimental and numerical characterization of an
452   impure phase change material using a thermal lattice Boltzmann method," *Appl Therm
453   Eng*, vol. 154, no. September 2018, pp. 738–750, 2019, doi:
454   10.1016/j.applthermaleng.2019.03.026.

455   [3]   R. Aridi and A. Yehya, "Review on the sustainability of phase-change materials used in
456   buildings," *Energy Conversion and Management: X*, vol. 15, p. 100237, Aug. 2022, doi:
457   10.1016/J.ECMX.2022.100237.

458   [4]   Q. Meng and J. Hu, "A poly(ethylene glycol)-based smart phase change material," *Solar*
459   *Energy Materials and Solar Cells*, vol. 92, no. 10, pp. 1260–1268, 2008, doi:
460   10.1016/j.solmat.2008.04.026.

461   [5]   Y. Ouchi, S. Someya, T. Munakata, and H. Ito, "Visualization of the phase change behavior
462   of sodium acetate trihydrate for latent heat storage," *Appl Therm Eng*, vol. 91, pp. 547–
463   555, 2015, doi: 10.1016/j.applthermaleng.2015.08.056.

464   [6]   R. R. Kasibhatla, A. König-Haagen, F. Rösler, and D. Brüggemann, "Numerical modelling of
465   melting and settling of an encapsulated PCM using variable viscosity," *Heat and Mass*
466   *Transfer/Waerme- und Stoffuebertragung*, vol. 53, no. 5, pp. 1735–1744, 2017, doi:
467   10.1007/s00231-016-1932-0.

468   [7]   J. Hirschey, K. R. Gluesenkamp, A. Mallow, and S. Graham, "Review of Inorganic Salt
469   Hydrates with Phase Change Temperature in Range of 5 ° C to 60 ° C and Material Cost
470   Comparison with Common Waxes," *5th International High Performance Buildings*
471   *Conference*, no. July, pp. 1–10, 2018.

472   [8]   M. Dannemand, J. M. Schultz, J. B. Johansen, and S. Furbo, "Long term thermal energy
473   storage with stable supercooled sodium acetate trihydrate," *Appl Therm Eng*, vol. 91, pp.
474   671–678, 2015, doi: 10.1016/j.applthermaleng.2015.08.055.

475   [9]   N. Xie, Z. Huang, Z. Luo, X. Gao, Y. Fang, and Z. Zhang, "Inorganic salt hydrate for thermal
476   energy storage," *Applied Sciences (Switzerland)*, vol. 7, no. 12, 2017, doi:
477   10.3390/app7121317.

478   [10]   G. G. D. Han, J. H. Deru, E. N. Cho, and J. C. Grossman, "Optically-regulated thermal energy
479   storage in diverse organic phase-change materials," *Chemical Communications*, vol. 54,
480   no. 76, pp. 10722–10725, 2018, doi: 10.1039/C8CC05919E.

481   [11]   G. G. D. Han, H. Li, and J. C. Grossman, "Optically-controlled long-term storage and release
482   of thermal energy in phase-change materials," *Nat Commun*, vol. 8, no. 1, 2017, doi:
483   10.1038/s41467-017-01608-y.

484   [12]   A. Kobayashi, M. Horikawa, J. L. Kirschvink, and H. N. Golash, "Magnetic control of
485   heterogeneous ice nucleation with nanophase magnetite: Biophysical and agricultural
486   implications," *Proc Natl Acad Sci U S A*, vol. 115, no. 21, pp. 5383–5388, 2018, doi:
487   10.1073/pnas.1800294115.

488   [13]   P. K. Jha, E. Xanthakis, V. Jury, and A. Le-Bail, "An overview on magnetic field and electric
489   field interactions with ice crystallisation; application in the case of frozen food," *Crystals*
490   *(Basel)*, vol. 7, no. 10, 2017, doi: 10.3390/cryst7100299.

[14] N. S. Bondareva, N. S. Gibanov, and M. A. Sheremet, "Computational study of heat transfer inside different PCMs enhanced by Al2O3 nanoparticles in a copper heat sink at high heat loads," *Nanomaterials*, vol. 10, no. 2, 2020, doi: 10.3390/nano10020284.

[15] K. Kant, A. Shukla, A. Sharma, and P. Henry Biwole, "Heat transfer study of phase change materials with graphene nano particle for thermal energy storage," *Solar Energy*, vol. 146, pp. 453–463, Apr. 2017, doi: 10.1016/J.SOLENER.2017.03.013.

[16] H. Li, C. Hu, Y. He, J. Zhu, H. Liu, and D. Tang, "A synergistic improvement in heat storage rate and capacity of nano-enhanced phase change materials," *Int J Heat Mass Transf*, vol. 192, p. 122869, Aug. 2022, doi: 10.1016/J.IJHEATMASSTRANSFER.2022.122869.

[17] C. Author, "PERFORMANCE MODELING OF A NOVEL ' SMART ' MAGNETIC PARTICLE-EMBEDDED PCM LAYER FOR THERMAL MANAGEMENT * Corresponding Author," no. July, pp. 1–7, 2018.

[18] E. Gonçalves, M. Faghri, Y. Asako, and M. Charmchi, "Numerical solution of melting processes for unfixed phase-change material in the presence of electromagnetically simulated low gravity," *Numeri Heat Transf A Appl*, vol. 46, no. 4, pp. 343–365, 2004, doi: 10.1080/10407780490478380.

[19] E. Yousefi, H. R. Nazif, H. Najafi Khaboshan, and A. Azarinia, "Non-Uniform Magnetic Field Effect on Forced Convection Heat Transfer of Flattened Tubes Using Two-Phase Mixture Model," *Heat Transfer Engineering*, vol. 42, no. 12, pp. 1041–1058, 2021, doi: 10.1080/01457632.2020.1766251.

[20] S. A. M. Mehryan, A. Tahmasebi, M. Izadi, and M. Ghalambaz, "Melting behavior of phase change materials in the presence of a non-uniform magnetic-field due to two variable magnetic sources," *Int J Heat Mass Transf*, vol. 149, 2020, doi: 10.1016/j.ijheatmasstransfer.2019.119184.

[21] A. Doostani, M. Ghalambaz, and A. J. Chamkha, "MHD natural convection phase-change heat transfer in a cavity: analysis of the magnetic field effect," *Journal of the Brazilian Society of Mechanical Sciences and Engineering*, vol. 39, no. 7, pp. 2831–2846, 2017, doi: 10.1007/s40430-017-0722-z.

[22] F. Selimefendigil and H. F. Öztop, "Impacts of magnetic field and hybrid nanoparticles in the heat transfer fluid on the thermal performance of phase change material installed energy storage system and predictive modeling with artificial neural networks," *J Energy Storage*, vol. 32, no. September, p. 101793, 2020, doi: 10.1016/j.est.2020.101793.

[23] A. Yehya, H. Naji, and L. Zalewski, "Experimental and numerical characterization of an impure phase change material using a thermal lattice Boltzmann method," *Appl Therm Eng*, vol. 154, pp. 738–750, May 2019, doi: 10.1016/j.applthermaleng.2019.03.026.

[24] A. Yehya and H. Naji, "Towards the simulation of supercooling and convection in phase change materials using a thermal lattice Boltzmann method," 2018.

[25]   A. D. Brent, V. R. Voller, and K. J. Reid, "Enthalpy-porosity technique for modeling convection-diffusion phase change: Application to the melting of a pure metal," *Numerical Heat Transfer*, vol. 13, no. 3, pp. 297–318, 1988, doi: 10.1080/10407788808913615.

[26]   B. Kamkari and H. J. Amlashi, "Numerical simulation and experimental verification of constrained melting of phase change material in inclined rectangular enclosures," *International Communications in Heat and Mass Transfer*, vol. 88, no. October, pp. 211–219, 2017, doi: 10.1016/j.icheatmasstransfer.2017.07.023.

[27]   A. Singh, A. Kumar, A. Kumar, N. Modelling, and M. Solidification, "OpenFOAM To cite this version : HAL Id : hal-02101324 OpenFOAM," 2019.

[28]   M. Rostami Dibavar, M. Mohammadpourfard, F. Mohseni, and S. Zeinali Heris, "Numerical study on the effect of non-uniform magnetic fields on melting and solidification characteristics of NEPCMs in an annulus enclosure," *Energy Convers Manag*, vol. 171, no. June, pp. 879–889, 2018, doi: 10.1016/j.enconman.2018.06.040.

[29]   M. Achparaki *et al.*, "We are IntechOpen , the world ' s leading publisher of Open Access books Built by scientists , for scientists TOP 1 %," *Intech*, p. 13, 2012, [Online]. Available: http://dx.doi.org/10.1039/C7RA00172J%0Ahttps://www.intechopen.com/books/advanced-biometric-technologies/liveness-detection-in-biometrics%0Ahttp://dx.doi.org/10.1016/j.colsurfa.2011.12.014

[30]   M. Faden, A. König-Haagen, and D. Brüggemann, "An optimum enthalpy approach for melting and solidification with volume change," *Energies (Basel)*, vol. 12, no. 5, 2019, doi: 10.3390/en12050868.

[31]   A. Yehya and H. Naji, "Thermal lattice Boltzmann simulation of entropy generation within a square enclosure for sensible and latent heat transfer," *Applied Sciences (Switzerland)*, vol. 5, no. 4, pp. 1904–1921, 2015, doi: 10.3390/APP5041904.

[32]   A. Yehya and H. Naji, "A Novel Technique to Analyze the Effect of Enclosure Shape on the Performance of Phase-change Materials," in *Energy Procedia*, 2015, vol. 75, pp. 2131–2136. doi: 10.1016/j.egypro.2015.07.344.

[33]   A. Yehya, H. Naji, and L. Zalewski, "Simulation numérique de la convection avec surfusion dans un matériau à changement de phase via la méthode de Boltzmann."

[34]   M. R. Mohaghegh, Y. Alomair, M. Alomair, S. H. Tasnim, S. Mahmud, and H. Abdullah, "Melting of PCM inside a novel encapsulation design for thermal energy storage system," *Energy Conversion and Management: X*, vol. 11, p. 100098, Sep. 2021, doi: 10.1016/J.ECMX.2021.100098.

[35]   M. Awais, M. Saad, H. Ayaz, M. M. Ehsan, and A. A. Bhuiyan, "Computational assessment of Nano-particulate (Al2O3/Water) utilization for enhancement of heat transfer with varying straight section lengths in a serpentine tube heat exchanger," *Thermal Science and Engineering Progress*, vol. 20, p. 100521, Dec. 2020, doi: 10.1016/J.TSEP.2020.100521.

566